Enhanced Electrical Properties of P3HT:WO_3 Hybrid Thin Film Transistors

Beyza Yedikardeş[1,*], Fereshteh Ordokhani[1], Nihat Akkan[2], Ece Kurt[3], Nilgün Karatepe Yavuz[4], Esra Zayim[3], Mustafa Altun[5]

[1] Department of Nano Science & Nano Engineering, Istanbul Technical University, Istanbul, Turkey

[2] Department of Electronics and Communication Engineering, Yıldız Tehnical University, Istanbul, Turkey

[3] Department of Physics Engineering, Istanbul Technical University, Istanbul, Turkey

[4] Institute of Energy, Istanbul Technical University, Istanbul, Turkey

[5] Department of Electronics and Communication Engineering, Istanbul Technical University Istanbul, Turkey

*Corresponding author: beyzayedikardes@gmail.com

Abstract

In recent decades, conjugated polymers have been widely studied in organic electronics to produce low-cost transistors. Additionally, these polymers are doped with inorganic materials in order to improve the transistor performance in terms of mobility, on/off current ratio, and threshold voltage as well as to ease processability. In this study, we use various doping concentrations (0-50% in weight) of tungsten oxide (WO_3) in poly(3-hexylthiophene) (P3HT), a well-studied organic semiconductor, to optimize the transistor performance. We treat spin-coated film of the hybrid P3HT:WO_3 solution on hexamethyl disilazane (HMDS) as channels of commercial test chips including 20 transistors with their gold electrodes.

Compared to using pristine P3HT, the proposed hybrid P3HT:WO_3 formula which significantly improves the transistor performance. Almost 105 times larger mobilities, almost 10 times larger on/off current ratios, and nearly 22 V decrease in threshold voltages were

achieved. It was also observed that the excess amount of WO_3 doping leads to worse mobilities and on/off current ratios.

Keywords

OFET, organic electronics, organic - inorganic hybrid thin films, P3HT, WO_3

1. Introduction

Conjugated polymers have drawn attention for several applications such as thin film transistors, optoelectronics, light emitting diodes and solar cells [1–4]. Organic polymers can be coated with vacuum-free, solution-based methods (such as spray coating, spin coating, dip coating...) at low temperatures which allow relatively cheaper fabrication that extends application areas. Although conventional silicon-based devices are very stable and have high mobility, they are not suitable for large scale applications. They also require high temperatures and expensive vacuum processes. Therefore, polymer-based devices are preferred for large area electronics. However, the vast majority of organic semiconductors exhibit worse transistor performance than inorganic semiconductors due to their low field effect mobility (μ_{FET}), on/off current ratio (I_{ON}/I_{OFF}) and threshold voltage (V_T). For instance, while the charge carrier mobility of silicon is > 1 $cm^2 V^{-1} s^{-1}$, the mobility of poly(3-hexylthiophene) (P3HT) -the most commonly used conjugated polymer- is in the range of 10^{-5}-10^{-1} $cm^2 V^{-1} s^{-1}$ [5], [6].

In order to improve electrical properties with a motivation that free charge carriers can be controlled by doping concentration, inorganic dopant molecules such as ZnO and TiO_2 can be added into the organic polymers [7–11]. Thus, it is possible to improve transistor parameters including threshold voltage, on/off current ratio, and field effect mobility. Navan and co-workers [12] increased field effect mobility of P3HT only 1.5 times for 40% of ZnO by weight in P3HT (from $1.15x10^{-3}$ up to $1.8x10^{-3}$ $cm^2 V^{-1} s^{-1}$). However, dispersing ZnO in P3HT solution did not affect on/off current ratio. In another work [9], ZnO nanorods were dispersed in P3HT and field effect mobility improved from $4x10^{-4}$ to $4x10^{-3}$ $cm^2 V^{-1} s^{-1}$. The on/off current ratio

remained the same for ZnO-P3HT composite devices and there was no significant change in threshold voltages.

Similar to ZnO and TiO_2, WO_3 is an *n*-type semiconductor having an adjustable wide band gap (E_g=2.5 – 3.2 eV) at room temperature, high electron affinity [13] and a remarkably high work function (Φ > 6 eV) [14–16]. Besides, WO_3 has very good electrochromic, photochromic and gas sensing properties and it is also used in ion sensing field effect transistors (ISFET) [17],[18]. The dual electrical effect of metal oxide-based transistors can be relevant for numerous applications, such as active-matrix electrochromic displays regardless of the transistor size. All these superior properties make WO_3 an attractive material in not only solid state sensor devices, but also the other areas of integrated circuit technology. Although theoretical study has been carried out on transition metal oxides used as dopant molecules, no previous study has experimentally assessed the doping of WO_3 into P3HT for transistor application.

The novelty of this study is to undertake WO_3 particles used as a dopant molecule by dispersing in P3HT/1,2-dichlorobenzene solution. Subsequently, WO_3 doped P3HT solutions were coated on prefabricated commercial chips to be tested for transistor performance. The present research explores, for the first time, the effects of WO_3 doping on transistor performance of P3HT thin films. Also, it is worth to say that the doping of P3HT with proper amount of WO_3 improves all device parameters.

Unlike similar studies in this field, not only electrical characterizations but also thin film characterizations were performed in details in order to explain the effect of WO_3 doping on both structural and physical properties. Besides, since both WO_3 [19] and P3HT [20] have electrochromic and gas sensing properties, this new hybrid formulation can be successfully and rewardingly used for electrochromic, transparent and flexible sensors and their electronic device applications such as self powered gas detection sensors [21–25].

2. Experimental

2.1 Chemicals

Poly(3-hexylthiophene-2,5-diyl) (P3HT, regioregular ≥90%, average M_w=25000-45000 g/mol, Sigma Aldrich), Hexamethyldisilazane (HMDS, purity >99%, Sigma Aldrich) were used as-received without any purification. 1,2-Dichlorobenzene (anhydrous, >99%, Sigma Aldrich) was used as organic solvent. Tungsten oxide particles (WO_3 powder) were used as dopant molecule [26] .

2.2 Transistor configuration

Pre-fabricated high density test chips with bottom-gate, bottom-contact (BGBC) structure were purchased from Ossila Ltd. Each test chip has 20 transistors, the highly *p*-doped silicon substrate with Au gate (G) electrode which covers the conductive edge of the substrate, the 300 nm–thick SiO_2 gate dielectric, and Au source (S) and drain (D) electrodes. The channel length (*L*) and channel width (*W*) of each transistor are 30 μm and 1 mm, respectively. Fig. 1 presents the top view of the test chip and the simplified schematic of a single BGBC transistor structure.

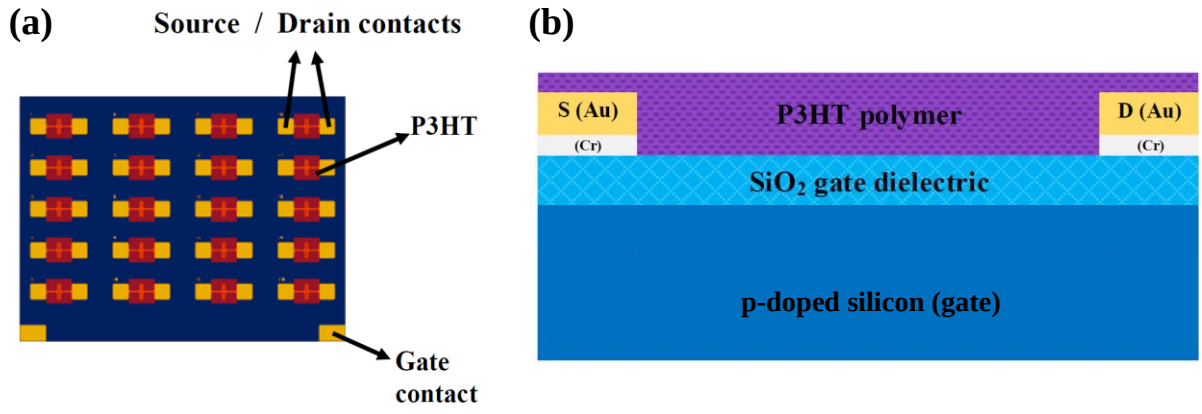

Fig. 1. (a) Top view of the pre-fabricated test chip [Image remains the copyright of Ossila Ltd. taken with permission from Ossila.com], (b) a simplified schematic drawing of BGBC structure. Note that Cr indicates the chromium adhesion layer and gate electrode which covers the conductive edge of the substrate is not shown for the sake of clarity.

2.3 Preparation of coating solutions

Since the interface cleaning of semiconducting layer is crucial for coating process and device performance, test chips have undergone a series of cleaning procedures. At first, 10 min ultrasonic cleaning was performed with isopropyl alcohol and 1,2-dichlorobenzene, respectively. Then, test chips were dried with nitrogen gun and treated with Uv-ozone for 10 min to remove excess amount of organic residues. After Uv-ozone cleaning, to reduce surface energy at the interface between semiconducting layer and SiO_2, HMDS was spin coated at 4000 rpm for 40 s and annealed for 5 min at 100°C. Since P3HT has a hydrophobic nature due to its long alkyl chain, it does not spread properly on the hydrophilic SiO_2 dielectric surface. In order to reduce surface energy at the interface and to increase wettability of P3HT solution on SiO_2, self-assembled monolayers such as alkyl silanes are coated between dielectric and semiconducting material [27–29]. In this work, hexamethyl disilazane (HMDS) was spin coated on SiO_2 prior to P3HT thin film coating. Besides, HMDS treatment prevents the charge trap formation at the interface and strongly affects the device performance [30],[31]. For the active layer, various concentrations of WO_3 (0 wt % , 10 wt %, 30 wt %, 40 wt %, 50 wt %) were dispersed in 10 mg P3HT/1 ml 1,2-dichlorbenzene solution by stirring overnight at 70°C. Both pure P3HT and WO_3 doped hybrid solutions were coated by spin coating over HMDS treated surface at 2500 rpm for 60 s and annealed for 30 min at 100°C. Source and drain contact pads and the rest of the chip surface except the channel region were gently wiped with a cotton swab to avoid short circuit. All solution preparation and coating process were carried out in inert glovebox ambient to avoid charge trap formation by oxygen and moisture. Table I shows the summary of the preparation recipe of coating solutions and nomenclature of the samples.

Table I Summary of coating recipe and sample nomenclature for both pure and hybrid coating solutions.

Sample Name	P3HT (mg)	1,2-dichlorobenzene (ml)	WO_3 (mg)	Doping concentration (wt %)
PW0 (pure)	10	1	-	0
PW10	10	1	1.1	10
PW30	10	1	4.3	30
PW40	10	1	6.6	40
PW50	10	1	10	50

2.4 Thin film and device characterization

The output and transfer characteristics of pure and WO_3 doped P3HT transistors were characterized by using Agilent B1500A Semiconductor Device Analyser. Three probes of analyser were used for three terminals of the transistors called source, drain, and gate. Structural and surface characterizations of the coatings were analysed using X-Ray Diffraction (XRD, Rikagu D/MAX-2200) with CuKα radiation within the range of 20-60° (2θ) and Scanning Electron Microscopy (SEM, Jeol JSM-6010LV, operated at 10kV under 500x magnification) and Electron Dispersive Spectroscopy (EDS) connected to SEM with Oxford software. Fourier Transform Infrared Spectroscopy (FTIR, Bruker) of the samples was performed in the wavenumber 400 cm^{-1} - 4000 cm^{-1} with the ATR plugin. Raman spectroscopy (Renishaw in Via Raman) was analysed under 532 nm laser excitation.

3. Results and discussion

3.1 Electrical characterization

Current–voltage (*I–V*) characteristics of the transistors were obtained by Agilent B1500A Semiconductor Parameter Analyzer under ambient conditions. The transfer characteristics were obtained by grounding the source terminal, applying voltage in the drain terminal, and

measuring the drain current while sweeping voltage of the gate terminal. On the other hand, the output characteristics were obtained similarly by grounding the source terminal, applying voltage in the gate terminal, and measuring the drain current while sweeping voltage of the drain terminal. Since the primary target was having threshold voltages as low as possible, the devices with the lowest V_T were selected and compared. Transfer characteristics of both pure P3HT and WO_3 doped P3HT hybrid samples are given in Fig. 2 and these characteristic curves are used to calculate some of the performance metrics such as threshold voltage, field effect mobility, and on/off current ratio. The gate-source voltage (V_{GS}) was swept from +40V to –40V in steps of –5V for each drain-source voltage (V_{DS}) stepped from 0 to –40V. Transfer characteristic curves of OFETs for both pure P3HT and WO_3 doped hybrid samples show the *p*-type and depletion mode behaviors. In these figures, it is seen that maximum drain-source current (I_{DS}) of P3HT was measured as 45nA and the doped samples provided higher I_{DS}, especially up to 3.3 μA for PW30 sample, compared to that of P3HT. On the other hand, output characteristics of the samples are presented in Fig. 3(a)-(e). The drain-source voltage was swept from 0 to –40V in steps of –2V for each gate-source voltage stepped from 40V to –40V in steps of –10V. When the V_{GS} was swept to –40V, *I-V* curves began to exhibit more linear behavior. Our measurement setup could not provide more than ± 40V supply voltage. Therefore, to be able to observe saturation behavior, a positive gate-source voltage close to the threshold voltage of PW30, e.g. V_{GS} = 10V, was applied instead of applying higher negative voltages in the drain terminal. The output characteristics of all samples are compared in Fig. 3(f) when V_{GS} = 10V. The saturation trend of the output curves can be clearly seen in this figure.

Transfer characteristic curves of the OFETs, obtained for V_{DS} = –40V, show quadratic behavior and therefore, threshold voltages and field effect mobilities of the OFETs were determined from these characteristic curves using the square-root expression of the conventional MOSFET

equation which is valid above threshold voltage and in saturation regime. This expression is given below:

$$\sqrt{|I_{DS}|} = \sqrt{\frac{1}{2}\mu_{FET} C_{ox} \frac{w}{L}} \times |(V_{GS} - V_T)| \quad (1)$$

where C_{ox} is the capacitance per unit area of gate oxide and its value is ~10.9 nF/cm^2.

The square root of I_{DS} is linearly dependent to the gate voltage. Hence, the linear extrapolation method in saturation region [32] was applied to extract threshold voltage. The square root of the measured data at V_{DS} = –40V was extrapolated to zero drain current and the interception point on the V_{GS}–axis gave us the V_T as shown in Fig. 4(a). The field effect mobility was calculated by the slope of the tangent line. On the other hand, maximum on/off current ratio is generally reported in the literature and it was calculated in this article from the measured transfer curves as given below:

$$\frac{I_{ON}}{I_{OFF}} = \frac{I_{DS}\,(V_{GS}=-40V, V_{DS}=-40V)}{I_{DS}\,(V_{GS}=+40V, V_{DS}=-40V)} \quad (2)$$

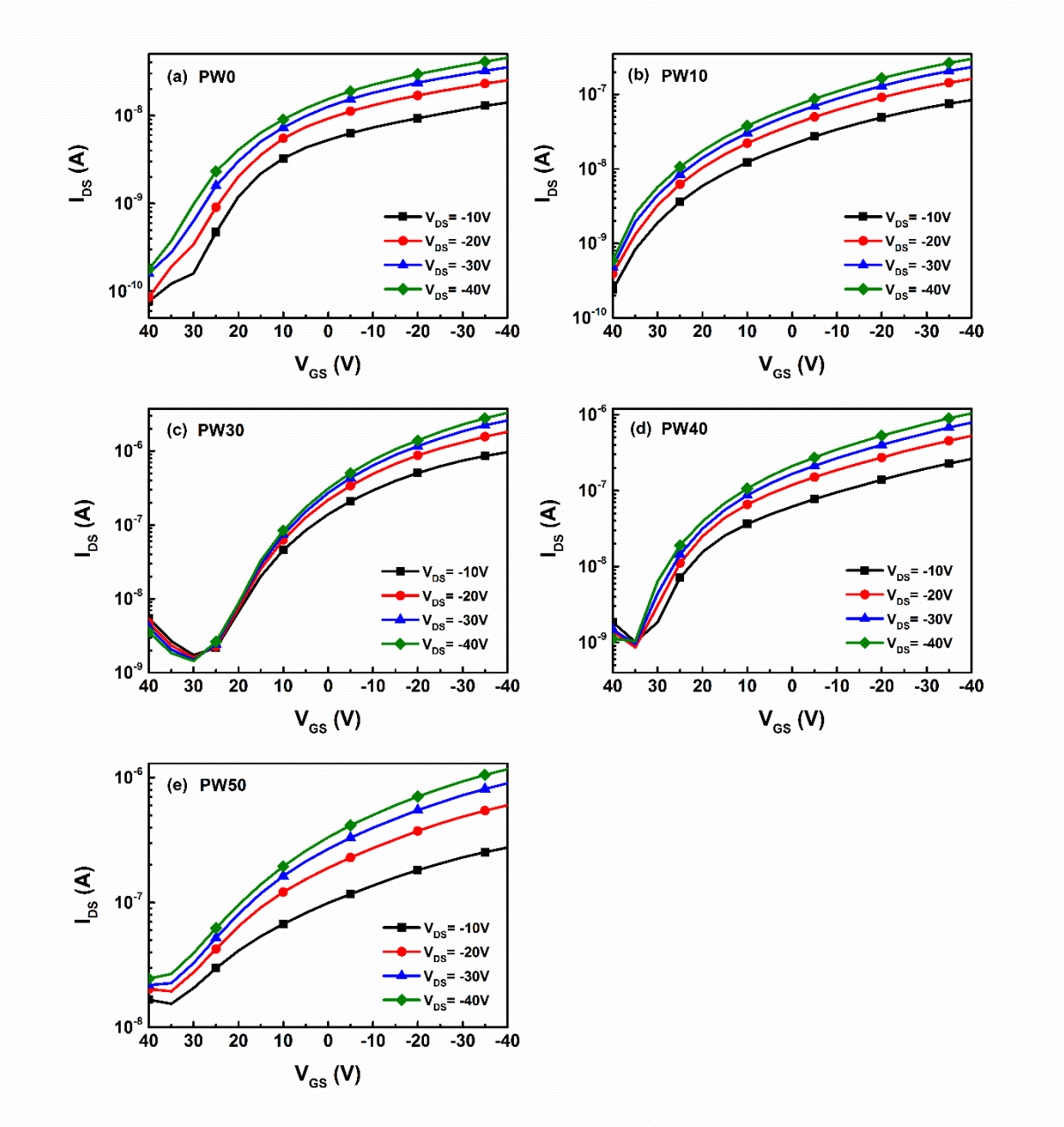

Fig. 2. Transfer characteristics of (a) PW0, (b) PW10, (c) PW30, (d) PW40, (e) PW50 OFETs.

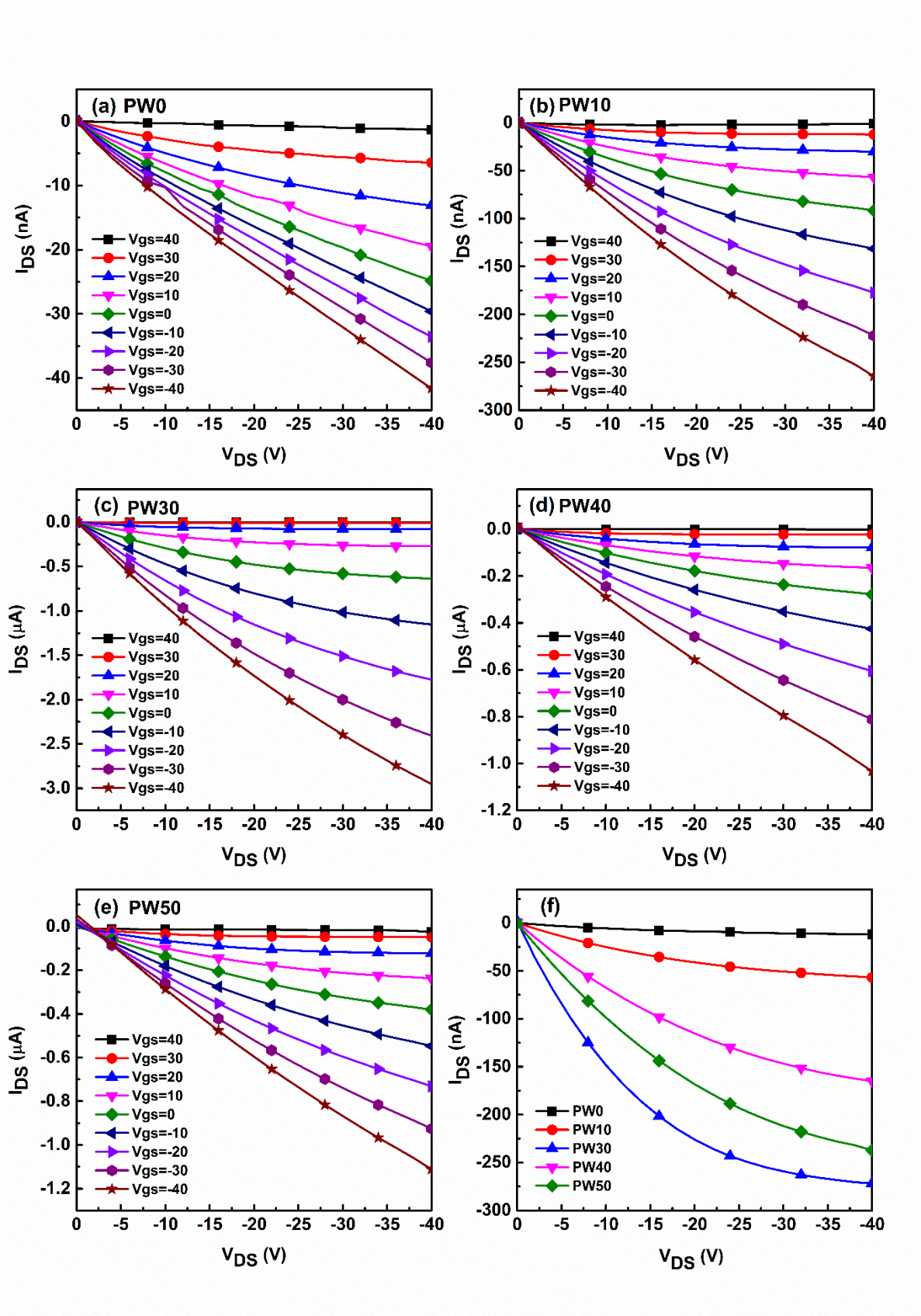

Fig. 3. Output characteristics of (a) PW0, (b) PW10, (c) PW30, (d) PW40, (e) PW50 OFETs, and (f) the comparison of output characteristics of pure P3HT and WO_3 doped P3HT hybrid OFETs when V_{GS} = 10V.

The calculated transistor parameters are given in Table II and plotted in Fig. 4. As it can be seen from Fig. 4(b), the on/off current ratio increases with the dispersion of WO_3 particles into the P3HT polymer until PW30. However, it starts to decrease when WO_3 concentration is increased further, since I_{ON} decreases and I_{OFF} increases for PW40 and PW50. Especially 50 wt % WO_3 makes the transistor always on within the operating voltage range and increases I_{OFF}. Moreover, field effect mobility increases up to PW30 with the increasing concentration of WO_3, particularly showing an enhancement almost 105 times for PW30 compared to that of PW0. The linearly extrapolated V_T is plotted in Fig. 4(d) and it is also improved from 40.1V to 17.7V. Figs. 4(b-d) also present error bars depicting the variations in these parameters for the other transistors on test chips. Similar enhancement trend is seen in these figures and the more efficient doping concentration of WO_3 is determined as 30 wt % in our experiments. As a summary, PW30 shows the best transistor performance among all.

Table II. Comparison of basic transistor parameters based on pure and WO_3 doped P3HT hybrid structures.

Sample Name	I_{ON}/I_{OFF}	μ ($cm^2 V^{-1} s^{-1}$)	V_T (V)
PW0	$2.5x10^2$	$5.3x10^{-5}$	40.1
PW10	$5.0x10^2$	$2.8x10^{-4}$	37.2
PW30	$2.3x10^3$	$5.6x10^{-3}$	17.7
PW40	$1.0x10^3$	$1.1x10^{-3}$	32.7
PW50	$5.0x10^1$	$9.0x10^{-4}$	45.1

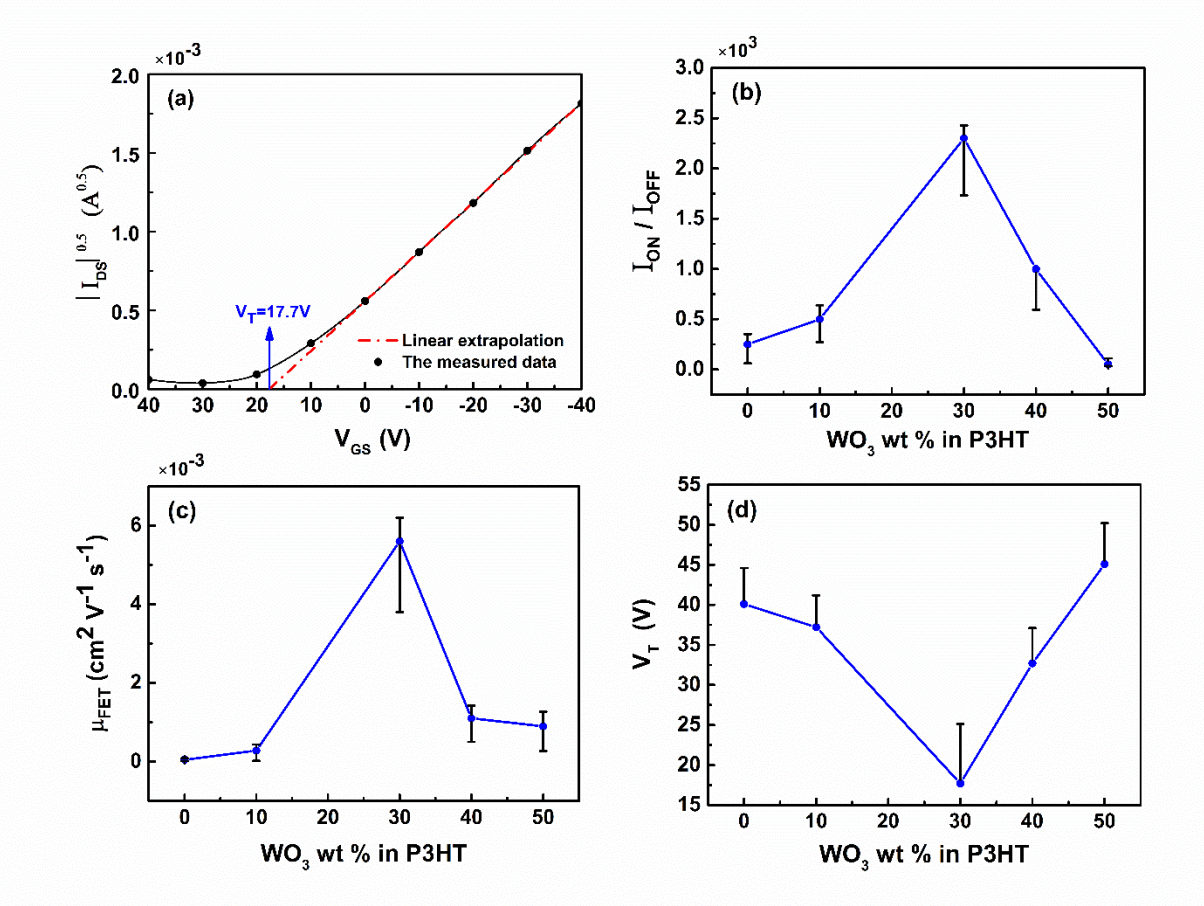

Fig. 4. (a) Implementation of linear extrapolation method in saturation region at V_{DS} = –40 V for PW30 data and summary of the effect of WO_3 doping concentration on (b) on/off current ratio, (c) field effect mobility, and (d) threshold voltage parameters. Error bars depict standard deviation over 10 devices.

3.2 Structural and chemical characterization

The energy dispersive x-ray spectroscopy (EDS) and elemental mapping analysis were performed. O, Si, S and W elements were identified for WO_3 doped P3HT coatings, indicating the definite presence of WO_3 and P3HT on the SiO_2 surface. As can be seen from Fig. 5, all doped formulations have well dispersion of WO_3 particles on the coating surface whereas PW0 has no WO_3 on the coating. It is clearly seen in Table III, when the doping concentration increases from PW10 to PW50, the amount of tungsten (W) increases, as well. However, it is observed that the WO_3 particles start to grow and agglomerate on the surface for PW50.

Table III. Elemental distribution of both pure and WO_3 doped P3HT hybrid coating solutions.

Sample Name	O %	Si %	S %	W %
PW0 (pure)	55.72	44.04	0.25	-
PW10	47.92	46.35	0.69	5.04
PW30	47.92	42.60	2.33	7.14
PW40	50.19	39.48	2.38	7.94
PW50	42.29	36.67	2.90	18.14

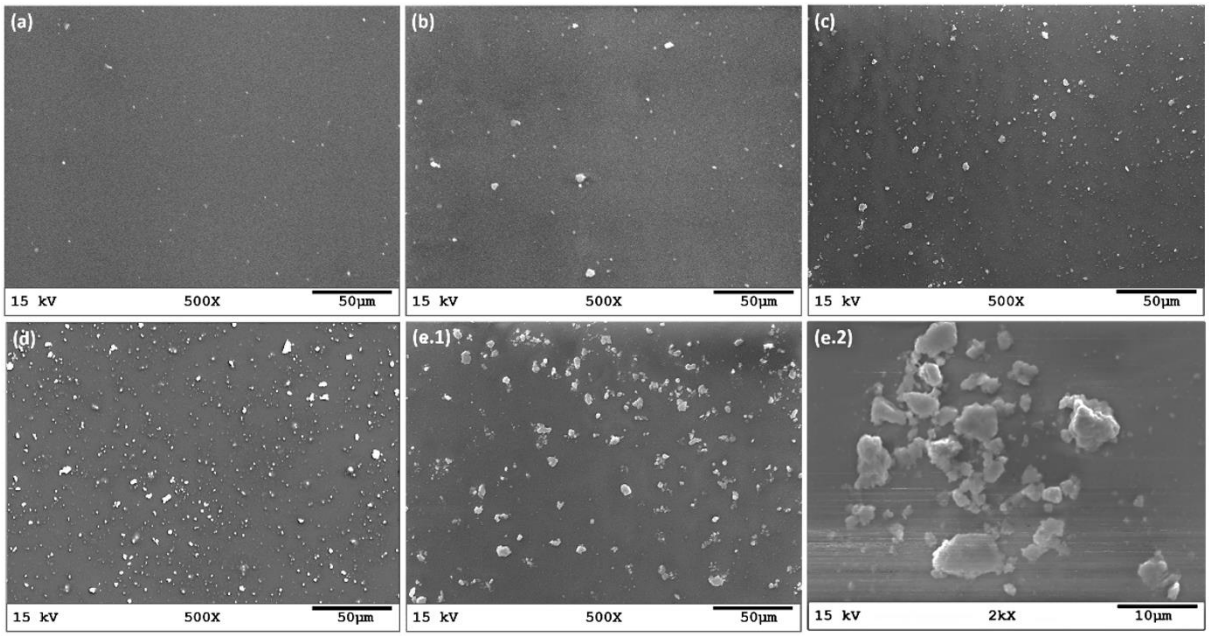

Fig. 5. SEM micrographs of (a) PW0, (b) PW10, (c) PW30, (d) PW40, and (e.1) PW50 coded samples at 500x magnification. (e.2) shows that the agglomerated WO_3 particles at 2000x magnification.

In order to investigate the effect of different amounts of WO_3 doping on electrical properties, only the samples which have the highest (PW30) and weakest (PW50) device performance were chosen and analysed for further chemical characterizations.

The crystalline structure of pure P3HT and WO_3 doped P3HT thin films were investigated by XRD. Scanning was performed over 2θ angles ranging from 20° to 60° to investigate characteristic peaks of both P3HT and WO_3 as seen in Fig. 6. Like many conjugated polymers, P3HT films show different crystal structures depending on the solvent type,

dissolution time, temperature and annealing conditions. Orientation, length and crystallinity degree is crucial for charge transport in the channel. In this study, pure P3HT shows a diffraction peak at $2\theta=23.4°$ due to the intermolecular $\pi \rightarrow \pi^*$ stacking corresponding to the (010) orientation [33], [34]. The distinct peaks of the XRD patterns exhibit at 2θ values of 23.16°, 28.04°, 33.93°, 36.79°, 47.44° and 49.90° correspond to (002), (020), (112), (022), (004) and (220) planes of hexagonal WO_3 (ICDD: 98-008-0635). After the doping of WO_3 particles, characteristic P3HT peak slightly shifts to $2\theta=23.6°$ due to some changes in interplane and interchain distances. Also, the peak becomes sharper which confirms improved crystallinity degree of P3HT. The appearance of prominent peak at $2\theta=28.04$ and other small peaks are attributed to the presence of WO_3 particles in the P3HT film. Considering the XRD spectrums, it can be estimated that there is a good interaction between polymer chains and WO_3 particles in PW30 due to the more effective crystallization than PW0.

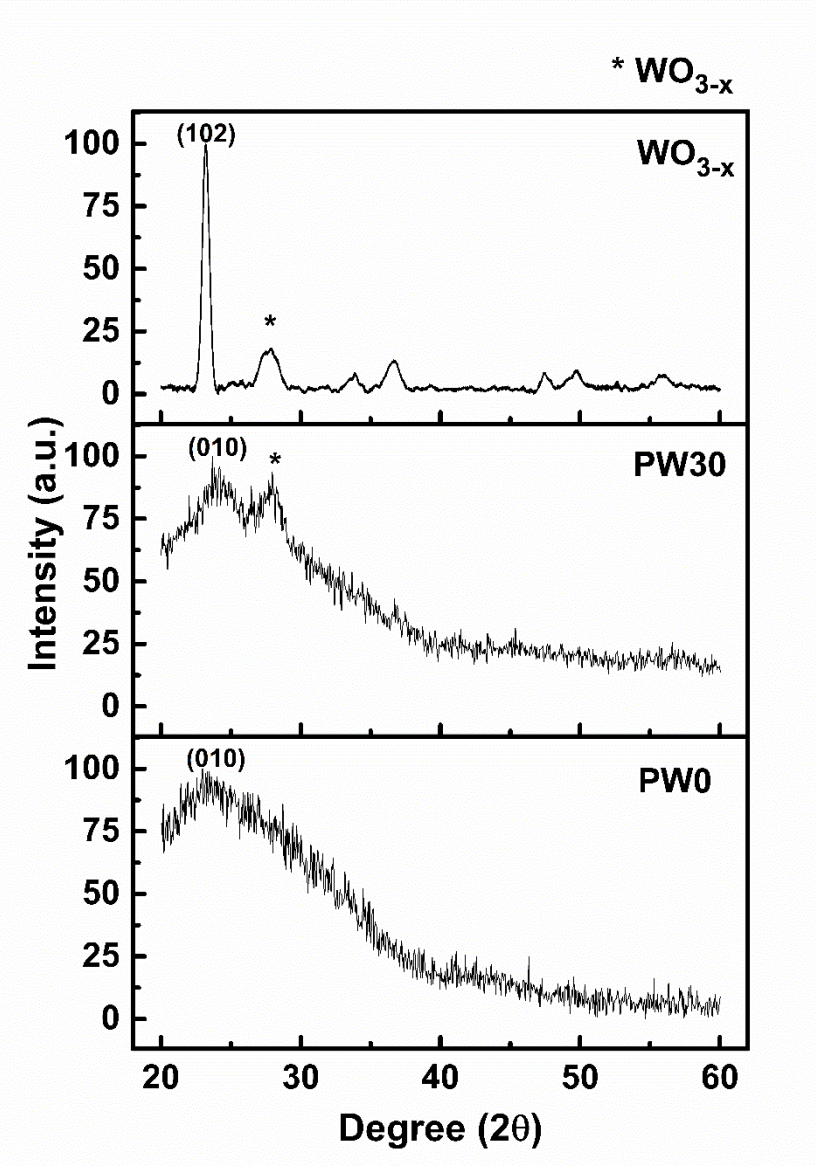

Fig. 6. XRD spectra of WO_3, PW0 and PW30 thin films.

Fig. 7 shows the FTIR spectrum of PW0, PW30 and PW50. It is observed that the spectrums between 500 and 3000 cm^{-1} wavenumbers indicate the fingerprint region for P3HT. The small peak at 3067 cm^{-1}, the intense peaks at 1573 cm^{-1} and 1456 cm^{-1} and the peak at 1252 cm^{-1} are assigned to C-H stretching vibrations, C=C stretching modes and C-C vibrations in thiophene unit of P3HT, respectively. The bands at 1126 cm^{-1} and 1033 cm^{-1} are due to the C-H_2 thiophene ring stretching vibrations. The characteristic C-S bands of P3HT appear at 943 cm^{-1}, 744 cm^{-1} and 657 cm^{-1}. The characteristic band located at 806 cm^{-1} wavenumber is attributed to W-O-W stretching vibration of WO_3 [35]. It is clearly seen that doping of WO_3

particles into the P3HT network does not lead any peak shifting since there is no covalent bonding. It is considered that WO_3 particles are attached to the P3HT polymer network with only electrostatic interactions. The absorption intensity of the peaks increases with the increasing content of WO_3 since the particles contribute to the system with extra absorption bands. These results verify that the P3HT polymer network is successfully incorporated with WO_3 particles.

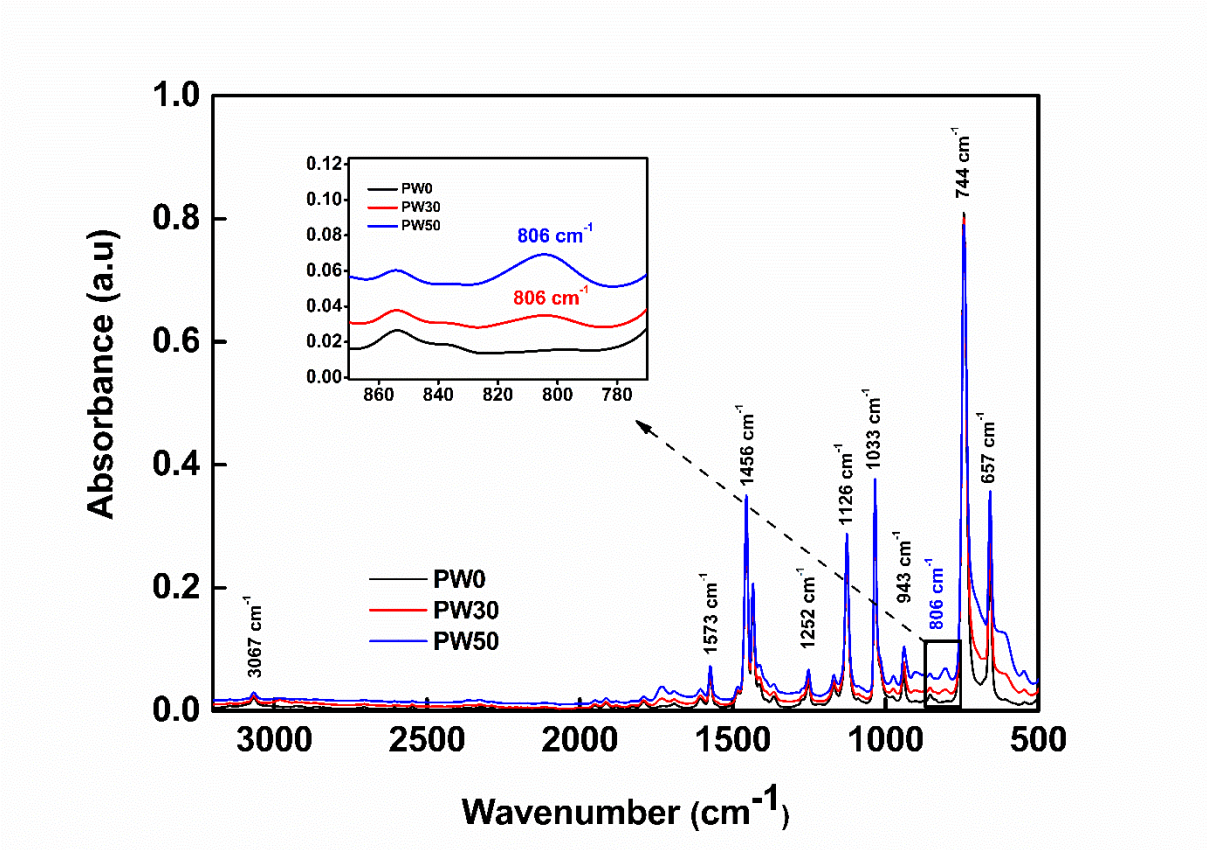

Fig. 7. FTIR spectrums of PW0, PW30 and PW50 thin films.

In order to investigate electrical interaction and structural properties of WO_3 doped films, Raman spectroscopy was performed. Raman spectrums at 600 – 1600 cm^{-1} wavenumbers are shown in Fig. 8. In the PW0 spectrum, Raman bands at 1452 cm^{-1} and 1097 cm^{-1} are assigned to C=C ring stretching and to C-H bending modes of inter rings, respectively. The small peak at 726 cm^{-1} of WO_3 doped thin films indicates the C-S-C deformation vibration and is supposed to be related to electron transfer between P3HT and WO_3. Furthermore, it is observed that the

C=C ring stretching peak at 1452 cm^{-1} shifts 6 cm^{-1} for PW30 while it shifts only 2 cm^{-1} for PW50. The peak intensity also increased after doping of WO_3 particles. The Raman shift towards lower wavenumbers refers that crystallinity degree of P3HT increases [36] with the doping of WO_3 particles and there is an effective conjugation throughout the polymer chain. Furthermore, Raman peak shifting can be approximated by following Hooke's Law equation;

$$\nu = \frac{1}{2\pi}\sqrt{\frac{k}{m^*}} \tag{3}$$

where ν is the frequency, k is the bond strength and m^* is the reduced mass. In this hybrid formulation, there is no covalent bonding between P3HT and WO_3 since WO_3 particles were only dispersed in the polymer solution by stirring. Therefore, it can be only referred to non-covalent interactions such as electrostatic cation- π or anion- π interactions, π- π stacking interactions and dispersion interactions. When P3HT was doped with the WO_3 particles, these particles can attach to the thiophene ring to take mobile π electrons from C=C double bonds or unpaired electron of sulphur element in the thiophene ring. Since the size of polymer fragments are very small compared to the size of WO_3 particles, it is assumed that WO_3 particles might interact with more than one thiophene unit along the polymer network. This coupling between polymer and WO_3 particles affects the molecular ordering and crystalline structure of P3HT chains due to the charge transfer efficiency. The schematic structure of the coupling between WO_3 and P3HT is simply shown in Fig. 9a.

Regarding Eq. 3, weakening the bond strength of thiophene chain causes a decrease in frequency. Since the wavenumber is directly proportional to the frequency, the Raman spectrum shifts to lower wavenumbers with the attachment of WO_3 particles. Exceeding the 30% of WO_3 by weight, the polymer chain is completely occupied with the excess amount of WO_3 particles and the particles cannot find any suitable place to bond and to transfer electrons. Consequently, Raman spectrum confirms that PW30 shows the best transistor performance due to the better interaction and electrical charge transfer with P3HT network.

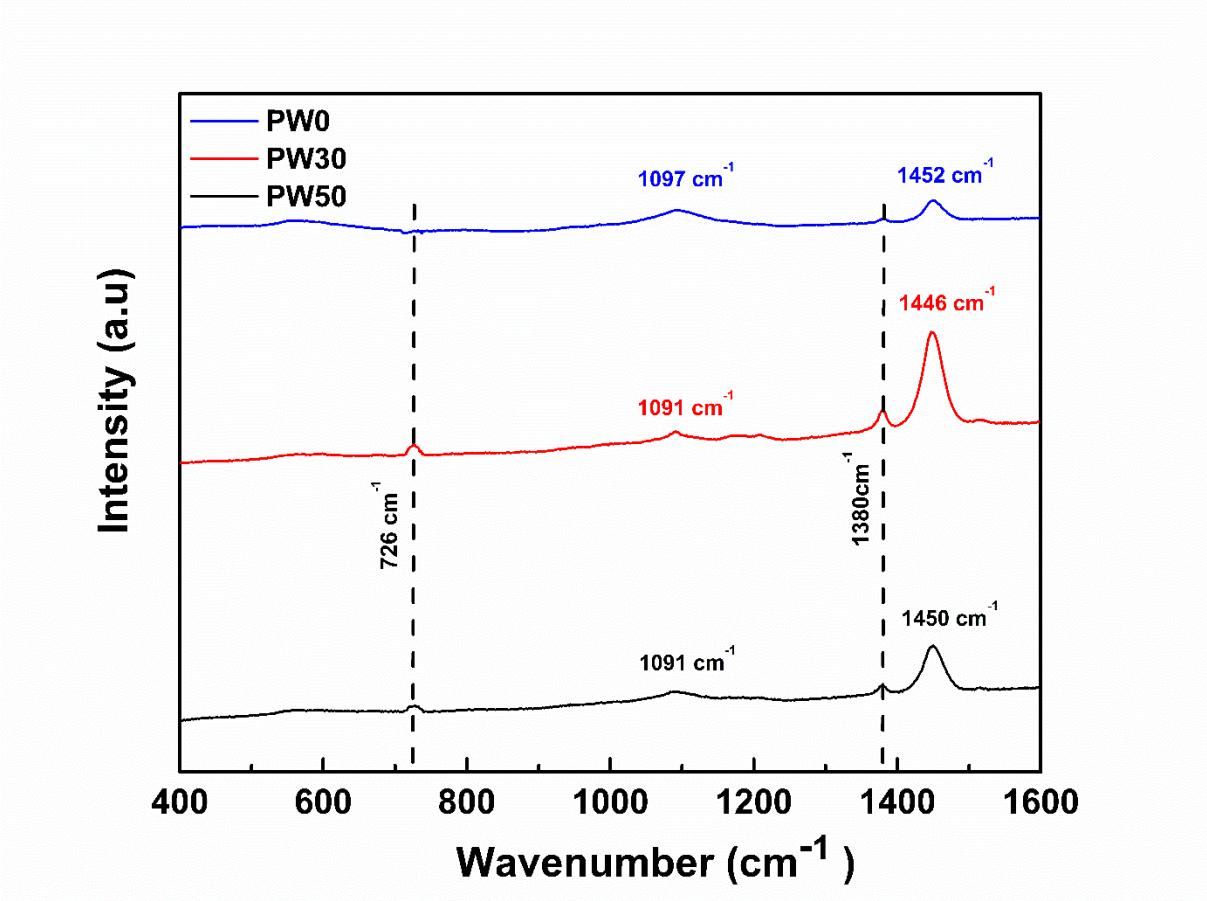

Fig. 8. Raman spectrums of PW0, PW30 and PW50 thin films.

The energy difference between conduction band of WO_3 and vacuum level is defined as electron affinity of WO_3 whereas the electron affinity of P3HT is defined as the energy difference between lowest unoccupied molecular orbital (LUMO) state of P3HT and vacuum level. The electron affinity of dopant molecule is responsible for the doping efficiency. Furthermore, when the highest occupied molecular orbital (HOMO) state of the polymer and the conduction band minimum energy level of dopant molecule are close to each other, effective doping can be carried out [37]. Since the electron affinity of WO_3 (E_{EA} > 4.5 eV) is higher than P3HT (E_{EA}≈3 eV) [38],[39], WO_3 particles tend to take electrons from the HOMO level of P3HT leaving behind the holes. This type of doping is called *p*-type doping [11] and the enhancement of hole carriers in P3HT is responsible for high channel mobilities. Also, it is suggested that the adequate WO_3 doping into P3HT increases mobility and reduces threshold

voltage, attributing to the passivation of trap states present in P3HT [40]. The charge transfer mechanism between WO_3 and P3HT is shown in Fig. 9b.

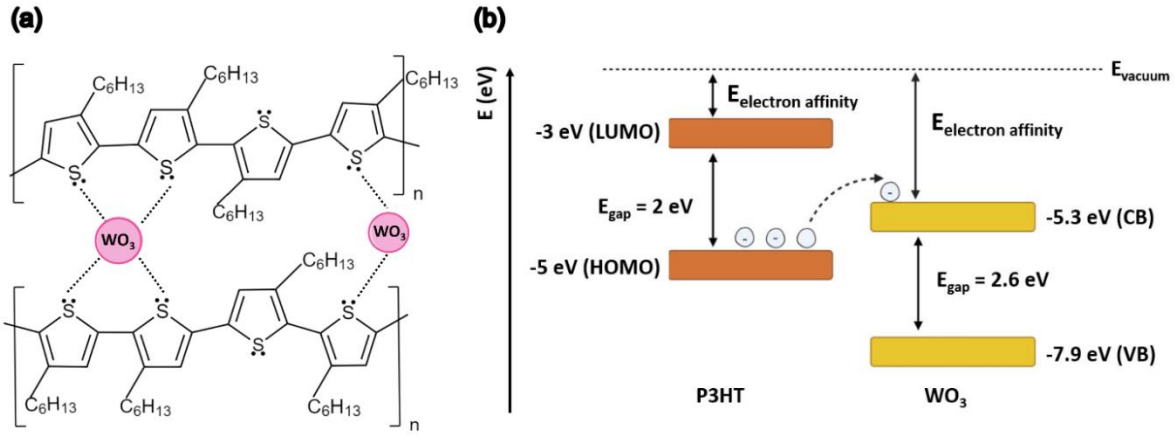

Fig. 9. Schematic illustration of (a) WO_3 doping into P3HT and (b) charge transfer between WO_3 and P3HT.

4. Conclusion

We achieved improvement in electrical performance of 3-polyhexylthiophene (P3HT) based thin film transistors by tungsten oxide (WO_3) doping using a very simple, single-step and room-temperature spin coating process. Different amounts of WO_3 were doped into P3HT and it was systematically studied to find the best transistor performance. We find that when the doping concentration is reached to 30% of WO_3 by weight in P3HT, μ_{FET} (from 5.3×10^{-5} cm^2 V^{-1} s^{-1} to 5.6×10^{-3} cm^2 V^{-1} s^{-1}) and I_{ON}/I_{OFF} (from 2.5×10^2 to 2.3×10^3) significantly increases. Also, V_T remarkably reduces (from 40.1V to 17.7V) via favorable charge-transfer doping and trap filling when compared to the undoped P3HT. XRD reveals that 30 wt % of WO_3 doping into P3HT generates new crystalline moieties on the P3HT-WO_3 hybrid chain resulting an increase in mobility. The observed changes in the intensity of fourier infrared spectrums and shifs of raman modes reveal that there is an excellent electrical charge transfer between P3HT and WO_3.

We believe that this systematical study and the results presented in this work will contribute to better understanding of doping mechanism in order to help fabrication of high performance transistors for flexible, solution-processed, low-cost, and large area electronics and chromogenics.

Acknowledgements

The authors would like to thank to Istanbul Technical University and The Scientific and Technological Research Council of Turkey (TUBITAK) for financial support. Also, the authors would like to thank Asst. Prof. Dr. Şeref Sönmez for WO_3 powders supply.

Author Contiributions

B.Y. and F.O. carried out the experiments. N.A performed the electrical characterization and calculations. E.K. drew the graphs. B.Y wrote the manuscript in consultation with E.Z and N.K. All authors discussed the results and commented on manuscript. M.A supervised the project.

Funding

This research was funded by The Scientific and Technological Research Council of Turkey (TUBITAK 1001 project) Nr. 116E250. Also, this work has been supported by the Scientific Research Projects realized at Istanbul Technical University, Nr. 41312.

Conflict of Interest

The authors declare that they have no conflict of interest.

References

1. R. C. Sanfelice, L. A. Mercante, A. Pavinatto, N. B. Tomazio, C. R. Mendonça, S. J. L. Ribeiro, L. H. C. Mattoso, and D. S. Correa, Hybrid composite material based on polythiophene derivative nanofibers modified with gold nanoparticles for optoelectronics applications. J. Mater. Sci. 52, 1919 (2017).

2. S. Savagatrup, A. D. Printz, D. Rodriquez, and D. J. Lipomi, Best of both worlds: conjugated polymers exhibiting good photovoltaic behavior and high tensile elasticity. Macromolecules

47, 1981 (2014).

3. T. P. Kaloni, P. K. Giesbrecht, G. Schreckenbach, and M. S. Freund, Polythiophene: from fundamental perspectives to applications. Chem. Mater. 29, 10248 (2017).

4. A. Marrocchi, D. Lanari, A. Facchetti, and L. Vaccaro, Poly(3-hexylthiophene): Synthetic methodologies and properties in bulk heterojunction solar cells. Energy Environ. Sci. 5, 8457 (2012).

5. S. Holliday, J. E. Donaghey, and I. McCulloch, Advances in charge carrier mobilities of semiconducting polymers used in organic transistors. Chem. Mater. 26, 647 (2014).

6. A. C. Arias, J. D. MacKenzie, I. McCulloch, J. Rivnay, and A. Salleo, Materials and applications for large area electronics: solution-based approaches. Chem. Rev. 11, 3 (2010).

7. T. Xie, G. Z. Xie, H. F. Du, Z. B. Ye, Y. J. Su, and Y. Y. Chen, The mobility improvement of organic thin film transistors by introducing ZnO-nanorods as an active layer. Sci. China Technol. Sci. 59, 714 (2016).

8. S. M. Mok, F. Yan, and H. L. W. Chan, Organic phototransistor based on poly(3-hexylthiophene)/TiO_2 nanoparticle composite. Appl. Phys. Lett. 93, 023310 (2008).

9. A. Kumar, R. R. Navan, A. Kushwaha, M. Aslam, And V. R. Rao, Performance enhancement of p-type organic thin film transistors using zinc oxide nanostructures. Int. J. Nanosci. 10, 761 (2011).

10. M. S. Hammer, C. Deibel, J. Pflaum, and V. Dyakonov, Effect of doping of zinc oxide on the hole mobility of poly(3-hexylthiophene) in hybrid transistors. Org. Electron. 11, 1569 (2010).

11. B. Lüssem, C. M. Keum, D. Kasemann, B. Naab, Z. Bao, and K. Leo, Doped organic transistors. Chem. Rev. 116, 13714 (2016).

12. R. R. Navan, B. Panigrahy, M. S. Baghini, D. Bahadur, and V. R. Rao, Mobility enhancement of solution-processed Poly(3-Hexylthiophene) based organic transistor using zinc

oxide nanostructures. Compos. Part B Eng. 43, 1645 (2012).

13. Y. Liu, J. Yu, and P. T. Lai, Investigation of WO_3/ZnO thin-film heterojunction-based schottky diodes for H_2 gas sensing. Int. J. Hydrogen Energy 39, 10313 (2014).

14. F. Wang, C. Di Valentin, and G. Pacchioni, Electronic and structural sroperties of WO_3: A systematic sybrid DFT study. J. Phys. Chem. C 115, 8345 (2011).

15. L. G. Gerling, S. Mahato, C. Voz, R. Alcubilla, and J. Puigdollers, Characterization of transition metal oxide/silicon heterojunctions for solar cell applications. Appl. Sci. 5, 695 (2015).

16. M. Mews, L. Korte, and B. Rech, Oxygen vacancies in tungsten oxide and their influence on tungsten oxide/silicon heterojunction solar cells. Sol. Energy Mater. Sol. Cells 158, 77 (2016).

17. R. C. De Campos, D. T. Cestarolli, M. Mulato, and E. M. Guerra, Comparative sensibility study of WO_3 ph sensor using EGFET and cyclic voltammetry. Mater. Res. 18, 15 (2015).

18. T. Onozato, Y. Nezu, H. J. Cho, and H. Ohta, Fast operation of a WO_3-based solid-state electrochromic transistor. AIP Adv. 9, 025122 (2019).

19. O. Gurcuoglu, D. Evecan, and E. Ozkan Zayim, Synthesis and characterization of tungsten oxide films by electrodeposition with various precursors and electrochromic device application. J. Solid State Electr. 19, 403 (2014).

20. T. Jiemsakul, K. Jiramitmongkon, U. Asawapirom, and C. Chotsuwan, Investigation of P3HT electrochromic polymer films prepared by ultrasonication of polymer solutions. J. Mater. Sci. 52, 8485 (2017).

21. T. H. Kim, H. J. Jeon, J. W. Lee, Y. C. Nah, Enhanced electrochromic properties of hybrid P3HT/WO_3 composites with multiple colorations. Electrochem. Commun. 57, 65 (2015).

22. J. Yang, G. Z. Xie, Y. J. Su, Q. P. Zhang, H. F. Du, H. L. Tai, X. S. Du, and Y. D. Jiang, Flexible organic thin-film transistors based on poly(3-hexylthiophene) films for nitrogen

dioxide detection. Sci. China Technol. Sci. 61, 1696 (2018).

23. S. Yuvaraja, A. Nawaz, Q. Liu, D. Dubal, S. G. Surya, K. N. Salama, and P. Sonar, Organic field-effect transistor-based flexible sensors. Chem. Soc. Rev. 49, 3426 (2020).

24. X. L. Liu, Y. Zhao, W. J. Wang, S. X. Ma, X. J. Ning, L. Zhao, and J. Zhuang, Photovoltaic self-powered gas sensing: A review. IEEE Sens. J. (Early Access) (2020).

25. J. Kim, J. H. Kim, and K. Ariga, Redox-active polymers for energy storage nanoarchitectonics. Joule 1, 739 (2017).

26. D. Evecan, S. Kaplan, M. Ş. Sönmez, S. Yıldırım, M. Okutan, H. Deligöz, and E. Zayim, Smart glass electrochromic device fabrication of uniform tungsten oxide films from its powder synthesized by solution combustion method. Microelectron. Eng. 215, 110989 (2019).

27. G. C. Schmidt, D. Höft, K. Haase, M. Bellmann, B. Kheradmand-Boroujeni, T. Hassinen, H. Sandberg, F. Ellinger, and A. C. Hübler, Fully printed flexible audio system on the basis of low-voltage polymeric organic field effect transistors with three layer dielectric. J. Polym. Sci. Part B Polym. Phys. 53, 1409 (2015).

28. W. Huang, W. Shi, S. Han, and J. Yu, Hysteresis mechanism and control in pentacene organic field-effect transistors with polymer dielectric. AIP Adv. 3, 052122 (2013).

29. G. Horowitz, R. Hajlaoui, H. Bouchriha, R. Bourguiga, and M. Hajlaoui, The concept of "threshold voltage" in organic field-effect transistors. Adv. Mater. 10, 923 (1998).

30. Y. Ito, A. A. Virkar, S. Mannsfeld, H. O. Joon, M. Toney, J. Locklin, and Z. Bao, Crystalline ultrasmooth self-assembled monolayers of alkylsilanes for organic field-effect transistors. *J.* Am. Chem. Soc. 131, 9396 (2009).

31. J. Zaumseil, P3HT and other polythiophene field-effect transistors. Adv. Polym. Sci. 265, 107 (2014).

32. D. K. Schroder, Semiconductor Material and Device Characterization, 3rd edn. (IEEE Press, Wiley, 2006) pp. 185-250.

33. A. Bolognesi, W. Porzio, A. Provasoli, C. Botta, A. Comotti, P. Sozzani, and R. Simonutti, Structural and thermal behavior of poly (3-octylthiophene): a DSC, ^{13}C MAS NMR, XRD, photoluminescence, and raman scattering study. Macromol. Chem. Phys. 202, 2586 (2001).

34. C. Borriello, S. Masala, V. Bizzarro, G. Nenna, M. Re, E. Pesce, C. Minarini, and T. Di Luccio, Electroluminescence properties of poly(3-hexylthiophene)-cadmium sulfide nanoparticles grown in situ. J. Appl. Polym. Sci. 122, 3624 (2011).

35. S. Li, P. Lin, L. Zhao, C. Wang, D. Liu, F. Liu, P. Sun, X. Liang, F. Liu, X. Yan, Y. Gao, and G. Lu, The room temperature gas sensor based on Polyaniline@flower-like WO_3 nanocomposites and flexible PET substrate for NH_3 detection. Sensors Actuators, B Chem. 259, 505 (2018).

36. D. E. Motaung, G. F. Malgas, C. J. Arendse, and S. E. Mavundla, Determination of the structure, morphology and complex refractive index in ZnO-nanopencils/P3HT hybrid structures. Mater. Chem. Phys. 135, 401 (2012).

37. B. Lüssem, M. Riede, and K. Leo, Doping of organic semiconductors. Phys. Status Solidi Appl. Mater. Sci. 210, 9 (2013).

38. J. C. Nolasco, R. Cabré, J. Ferré-Borrull, L. F. Marsal, M. Estrada, and J. Pallarès, Extraction of poly (3-hexylthiophene) (P3HT) properties from dark current voltage characteristics in a P3HT/n-crystalline-silicon solar cell. J. Appl. Phys. 107, 044505 (2010).

39. C. C. Chen, W. H. Chang, K. Yoshimura, K. Ohya, J. You, J. Gao, Z. Hong, and Y. Yang, An efficient triple-junction polymer solar cell having a power conversion efficiency exceeding 11%. Adv. Mater. 26, 5670 (2014).

40. S. Olthof, S. Singh, S. K. Mohapatra, S. Barlow, S. R. Marder, B. Kippelen, A. Kahn, Passivation of trap states in unpurified and purified C60 and the influence on organic field-effect transistor performance. Appl. Phys. Lett. 101, 253303 (2012).